arXiv:1304.2160v1 [cond-mat.mes-hall] 8 Apr 2013

Electronic temperature effect on the optical properties of spheroidal metal nanoparticles

Nicolas I. Grigorchuk *
Bogolyubov Institute for Theoretical Physics, National Academy of Sciences of Ukraine,
14-b Metrologichna Street, Kyiv-143, Ukraine, 03680

(Dated: April 9, 2013)

The effect of the electron temperature on both the light absorption and the scattering by metal nanoparticles (MNs) with excitation of the surface plasmon electron vibrations are studied in the framework of the kinetic theory. The formulae for the electroconductivity and polarisability tensors are derived for finite temperatures of an electron gas. The electrical conductivity and the halfwidth of the surface plasmon resonance are studied in detail for a spherical MN. Depending on the size of MN, the efficiencies of the light absorption and scattering with temperature changing are investigated. It is found, in particular, that the absorption efficiency can not only increased with a temperature decreasing, but decreases as well. Derived formulas allow to calculate analytically the various optical and transport phenomena for MNs with any spheroidal shape embedded in any dielectric media.

PACS numbers: 78.67.-n; 52.25.Os; 65.80.-g; 68.49.Jk; 73.23.-b

I. INTRODUCTION

When the metal nanoparticle is illuminated with a laser beam by frequency which coincides with the frequency of collective electron oscillations in the MN, the surface plasmon resonance (SPR) is excited. The frequency and the width of SPR depends on the size, morphology, spatial orientation of MN and on the dielectric environment.[1,2] Resonance light scatterers are employed in wide range applications ranging from surface enhanced Raman scattering,[3] near-field scanning optical microscopies,[4] to bio-chemistry imaging,[5] surface enhanced fluorescence,[6] subwavelength optical waveguides,[7] cancer therapy[8] etc.

The temperature effect on the optical and transport properties of the metal nanoparticles is very important for pure and applied science of the nanoparticles.[9] As a MN absorbs laser energy in a thin-surface layer, rapid local heating can occur at the surface. Thus, for a detailed analysis of the laser-light absorption or reflection at MN surfaces, the properties of MNs at electron temperatures must be studied. The temperature dependence of the SP resonance is crucial due to the number recent applications of noble MNs in computer chips,[10] thermally assisted magnetic recording,[11] thermal cancer treatment,[12] and catalysis and nanostructure growth.[13] The use of nano-objects as temperature sensors[14] and thermometers[15] is promising due to their small sizes and short thermal relaxation time.

Previous calculations the effect of the temperature on the different properties of the MNs were performed in the zero-temperature limit[16,17] or in the interval 15–1000 K only.[9,18–27] While the optical properties of both the bulk metals[28–32] and the MNs in the low-temperature regime is now well studied, an understanding of the effects of electron temperature (typically of order $10^4 K$) on the plasmon modes has remained a challenge and is not as well understood as at the $T = 0$. Such an out-of-equilibrium situation can easily be induced in metallic nanoparticles[33] using ultrashort optical pulses. At time $t = 0$, only the electrons are excited by the laser pulse; then the excited electron would decay through light radiation, phonon excitation, and/or electron-electron scattering. In the most commonly used approach, the two-temperature model,[31,34,35] which is assumed that both electronic and ionic degrees of freedom are in thermal equilibrium conditions individually, but each degree of freedom has its own temperature. The energy exchange between the electrons and the lattice in this model lead to a time-dependent electronic temperature $T_e(t)$.

The effect of electron temperature was not studied in detail to date because a broad temperature interval requires a usage of materials with high thermal stability. In Ref. 22,27 the improved Drude model when the electron concentration and/or a plasma frequency are directly dependent on the electron temperature were used. Only few works have so far addressed this problem.[36,37]

In this work, we focus on optical properties of metal nanoparticles at relatively high electron temperatures, whereas the ion temperature, T_i, is supposed to be much smaller.[33] Different behavior with temperature of optical lines for MNs with different radii and shapes are a particular motivation for our present study. The screening coming from the surrounding matrix is taken into account through a constant dielectric function, ϵ_m.

To calculate the effect of the electron temperature on the optical and transport characteristics of MNs, we will use the kinetic theory method which accounts for the electron scattering on the MN boundary. It is shown that the efficiency of absorption with temperature strongly depends on the size of MN. It is predicted that the effect of temperature on the MNs with different radii accounts for most of the possible optical properties in this interesting temperature regime. We present our theoretical results on the temperature dependence of the conductivity and polarizability tensors related to the MNs with the spheroidal shape.

---

*email: ngrigor@bitp.kiev.ua

The rest of the paper is organized as follows. The Boltzmann equation approach to the problem is presented in Sec. II. Section III contains the study of the conductivity tensor in the spheroidal MNs at finite temperatures. In Sec. IV, we consider the effect of temperature on the polarizability of MN. Section V is devoted to study of the light absorption and scattering crossection by MNs. The discussion of the obtained results is available in Sec. VI, and Sec. VII contains the conclusions.

II. BOLTZMANN EQUATION

To account for the temperature effect on the conductivity and polarization properties of the MNs, we will apply the Boltzmann equations approach. The advantages of this approach is that the obtained results can be applied not only to MNs with a spherical shape, but to strongly anisotropic spheroidal (needle-like or disk-shaped) MNs. Thus, it permits one to study the effect of the particle shape on the measured physical values. Second, the Boltzmann equation method enable us to investigate the MNs with sizes smaller than the electron mean free path l. But in the case of sizes less than l, it gives the same results as known from other approaches.

There exists a lower limit of the applicability of Boltzmann method in the small radius limit when the particle size is comparable to the de Broglie wavelength of the electron, and the quantization of the electron spectrum starts to play an essential role.[38] Practically, it is around a radius of greater or less than 2 nm.

Let us consider the single ellipsoidal metal MN with semiaxes a, b, c that is irradiated by an electromagnetic (EM) wave, whose electric field is given as

$$\mathbf{E} = \mathbf{E}_0 \exp[i(\mathbf{kr} - \omega t)]. \tag{1}$$

Here $\mathbf{E}_0$ is the amplitude of an electric field of a pump laser, ω is its frequency, $\mathbf{k}$ is the wave vector, and $\mathbf{r}$ and t describe the spatial coordinates and time.

We limit ourselves with the case of Rayleigh scattering, when the electromagnetic wavelength (from a pump laser) $\lambda \sim c/\omega$ is much larger than the diameter of the nanoparticle d $(= max\{a, b, c\})$. Then the electromagnetic field around the MN can be considered as homogeneous. Placing the coordinate origin in the center of the particle, the above-mentioned assumption is written as

$$kr \ll 1. \tag{2}$$

The inequality (2) implies that the $\mathbf{E}$ field of the electromagnetic wave can be considered to be spatially uniform on scales of the order of a particle size such that all the conduction electrons move in-phase producing only dipole-type oscillations. The amplitude of such a field is connected to $\mathbf{E}_0$ by the relation[39]

$$E_0^{(j)}(0, \omega)/E_{in}^{(j)}(\omega) = 1 + L_j[\epsilon(\omega)/\epsilon_m - 1], \tag{3}$$

where $\epsilon(\omega)$ is the dielectric permittivity of the MN, ϵ_m is the dielectric constant of the adjacent medium (i.e., solvent), and L_j are depolarization factors in the j-th direction (in the principal axes of an ellipsoid).

The electric field E_{in} gives rise to high-frequency current inside the MN. To obtain the average density of this current over the MN, it is necessary first of all to calculate the electron velocity distribution function. The field E_{in} has an effect on the equilibrium electron velocity distribution and thus determines the appearance of a nonequilibrium addition $f_1(\mathbf{r}, \mathbf{v}, t)$ to the Fermi distribution function

$$f_0(\varepsilon) = \frac{1}{\exp\left[\frac{\varepsilon - \mu(T)}{k_B T}\right] + 1}.$$

Here $\mu(T)$ is the chemical potential at finite temperature T, k_B is Boltzmann's constant, $\varepsilon = mv^2/2$ denotes the kinetic energy of an electron, $v = |\mathbf{v}|$ refers to the electron velocity, and m is the electron mass. As is well known,[40] the equilibrium function $f_0(\varepsilon)$ does not give any input to the current. Accounting for both the time dependence of Eq. (1) and the inequality (2), the total distribution function of electrons, can be represented as

$$f(\mathbf{r}, \mathbf{v}, t) = f_0(\varepsilon) + f_1(\mathbf{r}, \mathbf{v}, t) \equiv f_0(\varepsilon) + f_1(\mathbf{r}, \mathbf{v})\, e^{i\omega t}. \tag{4}$$

The function $f_1(\mathbf{r}, \mathbf{v})$ we will seek as a solution of the linearized Boltzmann's equation

$$(\nu - i\omega) f_1(\mathbf{r}, \mathbf{v}) + \mathbf{v}\frac{\partial f_1(\mathbf{r}, \mathbf{v})}{\partial \mathbf{r}} + e\mathbf{E}_{in}\mathbf{v}\frac{\partial f_0(\varepsilon)}{\partial \varepsilon} = 0, \tag{5}$$

where e is the electron charge. In Eq. (5) we have assumed that the collision integral

$$(\partial f_1/\partial t)_{col} = -f_1/\tau$$

is evaluated in the relaxation time approximation ($\tau = 1/\nu$, ν refers to electron collision frequency). Strictly speaking, $\nu \equiv \nu(T)$ is temperature dependent value which can be presented as

$$\nu(T) = \frac{n_e e^2}{m}\frac{K}{\Theta}\left(\frac{T}{\Theta}\right)^5 \int_0^{\Theta/T} \frac{z^5 e^z}{(e^z - 1)^2}\, dz, \tag{6}$$

where n_e is the electron concentration, Θ is the Debye temperature, and K combines together factors depending on the details of the Fermi surface geometry and scattering matrix elements.

For simplicity, we assume as well that the vortex electric field, induced by magnetic component of the external EM field, gives comparatively small input at the plasmon resonance frequencies and can be neglected in Eq. (5).

What is more, the function $f_1(\mathbf{r}, \mathbf{v})$ ought to satisfy the boundary conditions as well. These conditions may be chosen from the character of electrons reflection from the inner walls of the MN. We will adopt, as is usually done, the assumption of diffusive electron scattering by the boundary of MN. Then the boundary conditions can be presented in the form

$$f(\mathbf{r},\mathbf{v})|_S = 0, \qquad \mathbf{v}_n < 0, \tag{7}$$

where $\mathbf{v}_n$ is the velocity of the component normal to the particle surface.

Along with diffusive scattering, the mirror boundary conditions at the nanoparticle surface were examined in the literature for electron scattering (see, e.g., Ref. 40). In this case, each electron is reflected from the surface at the same angle at which it falls to the surface. In diffuse reflection, the electron is reflected from the surface at any angle. In order for the mirror mechanism to be dominant, the surface must be perfectly smooth in the atomic scale, since the degree of reflectivity of the boundary essentially depends on its smoothness. Practically, for a nonplanar border such smoothness is extremely difficult to achieve. As was shown,[41] the mirror boundary conditions give a small correction to the results obtained with the account of only the diffusive electron reflections. Therefore, we chose more realistic boundary conditions given by Eq. (7).

The boundary conditions (7) in the case of an ellipsoidal MN, generally speaking, depend on angles, what complicates the solution of Eq. (5).

It is rather easy to solve Eq. (5) and to satisfy the boundary conditions of Eq. (7) if one passes to the transformed coordinate system, where an ellipsoid with semi-axes a, b, c (along the x, y, and z directions, respectively) transforms into a sphere of radius R with the same volume:

$$x_j = \frac{d_j}{R} x'_j, \qquad R = (abc)^{1/3}, \tag{8}$$

with $j = 1, 2, 3$, and $d_1 = a$, $d_2 = b$, $d_3 = c$. A similar transformation should be made for the electron velocities:

$$\upsilon_j = \frac{d_j}{R} \upsilon'_j. \tag{9}$$

Equation (5) and the boundary conditions (7) in transformed coordinate and velocity systems, can be rewritten as

$$(\nu - i\omega) f_1(\mathbf{r}',\mathbf{v}') + \mathbf{v}' \frac{\partial f_1(\mathbf{r}',\mathbf{v}')}{\partial \mathbf{r}'} + e\mathbf{E}_{in}\mathbf{v}' \frac{\partial f_0(\varepsilon)}{\partial \varepsilon} = 0, \tag{10}$$

$$f(\mathbf{r}',\mathbf{v}')|_{r'=R} = 0, \qquad \mathbf{r}'\mathbf{v}' < 0. \tag{11}$$

The first condition calls for zero equality of the electron distribution function at the nanoparticle surface, and the second one, $\mathbf{r}'\mathbf{v}' < 0$, means that an electron motion occurs only inside MN and the electron leakage through the NP surface is absent.

Eq. (10) presents the partial differential equation with the boundary conditions (11). Using method of characteristics, one can obtain the solution to this equation in the form

$$f_1(\mathbf{r}',\mathbf{v}',t) = -e\frac{\partial f_0}{\partial \varepsilon} \mathbf{v}'\mathbf{E}_{in} \frac{1 - \exp[-(\nu - i\omega)\, t_c(\mathbf{r}',\mathbf{v}')]}{\nu - i\omega}, \tag{12}$$

where the characteristic $t_c(\mathbf{r}',\mathbf{v}')$ can be presented as

$$t_c(\mathbf{r}',\mathbf{v}') = \frac{1}{\mathbf{v}'^2} \left[\mathbf{r}'\mathbf{v}' + \sqrt{(\mathbf{R^2} - \mathbf{r}'^\mathbf{2})\, \mathbf{v}'^\mathbf{2} + (\mathbf{r}'\mathbf{v}')^\mathbf{2}} \right]. \tag{13}$$

The radius vector $\mathbf{R}$ determines the starting position of an electron at the moment $t_c = 0$. The characteristic curve of Eq. (13) depends only on the absolute value of $\mathbf{R}$ and does not depend on the direction of $\mathbf{R}$.

It is reasonable to point out here that, in spite of the electric field remains spatially uniform inside the MN, the distribution function Eq. (12) depends all the same on the coordinates in consequence of the requirement to obey boundary conditions Eq. (11). Owing to this dependence, other physical parameters averaged with $f_1(\mathbf{r}',\mathbf{v}')$ start to depend on coordinates too. Because, the physical sensing have only parameters averaged over whole MN volume V, it is necessary to fulfill the integration over all coordinates inside of MN. One can see this on the example just below.

Using the solution (12), one can calculate the density of a high-frequency current induced by the EM wave inside the MN. Performing the Fourier transformation of Eq. (12), we obtain

$$\mathbf{j}(\omega) = \frac{2e}{V} \left(\frac{m}{2\pi\hbar}\right)^3 \iiint\limits_V d^3r' \iiint d^3\upsilon'\, \mathbf{v}' f_1(\mathbf{r}',\mathbf{v}',\omega). \tag{14}$$

III. ELECTRIC-CONDUCTIVITY TENSOR

Let us introduce the tensor of electric conductivity $\sigma_{\alpha\beta}(\omega)$ using the relationship

$$j_\alpha(\omega) = \sum_{\beta=1}^{3} \sigma_{\alpha\beta}(\omega)\, E_{in}^{(\beta)}(\omega). \tag{15}$$

Then, in accordance with both Eqs. (12) and (14), the components of this tensor can be presented as

$$\begin{aligned} \sigma_{\alpha\beta}(\omega) \ &= -\frac{2e}{V}\left(\frac{m}{2\pi\hbar}\right)^3 \iiint\limits_V d^3r' \iiint d^3\upsilon'\ \upsilon_\alpha \\ \times \quad & \left(e\upsilon_\beta \frac{\partial f_0}{\partial \varepsilon} \frac{1 - e^{-(\nu - i\omega)t_c(r',\upsilon')}}{\nu - i\omega} \right). \end{aligned} \tag{16}$$

Electric-conductivity tensor $\sigma_{\alpha\beta} = \sigma_{\beta\alpha}$ is the symmetrical second-rank tensor. Because the integrand in Eq. (16)

is an odd function for a nondiagonal tensor components $\alpha \neq \beta$, and the integration is conducting over the whole velocity space $[-\infty, \infty]$, that retain only diagonal components in this equation.

If we introduce a rectangular coordinate system and chose the fundamental directions x, y, z to be coincident with the three principal axes of the ellipsoids then we get

$$\sigma = \begin{pmatrix} \sigma_{xx} & 0 & 0 \\ 0 & \sigma_{yy} & 0 \\ 0 & 0 & \sigma_{zz} \end{pmatrix}.$$

The tensor of electric conductivity, as can see from Eq. (16), is the complex value:

$$\sigma_{\alpha\beta}(\omega) = \sigma'_{\alpha\beta}(\omega) + i\sigma''_{\alpha\beta}(\omega). \qquad (17)$$

The surface effect on the conducting phenomenon is described in Eq. (16) by means of the characteristic $t_c(\mathbf{r}', \mathbf{v}')$. It accounts for the restrictions imposed on the electron movement by a nanoparticle surfaces. As one can see from Eq. (12), the value of t_c is of the order of $t' \sim R/\upsilon_F$, where υ_F is the Fermi velocity. This implies that the value reciprocal to t_c will correspond to the vibration frequency between the particle walls. Hence, the inequality $\nu t_c \gg 1$ indicates that the electron collision frequency inside the MN bulk would significantly exceed the one for an electron collision with the surface of MN. If this inequality is satisfied, one can to direct $t_c \to \infty$. Then the exponent in Eq. (16) vanish and finally we arrive at a standard expression for an electric-conductivity, such as following[1,39]

$$\sigma(\omega) = \frac{1}{4\pi} \frac{\omega_{pl}^2}{\nu - i\omega}, \qquad (18)$$

with

$$\omega_{pl}^2 = \frac{4e^2 m^2 \upsilon_F^3}{3\pi\hbar^3}. \qquad (19)$$

To ensure that, it is necessary to take into account that the energy derivative of f_0 in the zero approximation in the small ratio of $k_B T/\varepsilon_F$ (ε_F is the Fermi energy) can be replaced by

$$\frac{\partial f_0}{\partial \varepsilon} \approx -\delta(\varepsilon - \varepsilon_F), \qquad (20)$$

and pass in Eq. (16) to the integration over υ in the spherical coordinate system

$$\iiint\limits_{-\infty}^{\infty} d^3\,\upsilon \to \int\limits_0^{2\pi} d\varphi \int\limits_0^{\pi} \sin\theta\, d\theta \int\limits_0^{\infty} \upsilon^2\, d\upsilon,$$

with the use of the formula

$$\int_0^\infty \upsilon^4\, \delta(\upsilon^2 - \upsilon_F^2)\, d\upsilon = \frac{\upsilon_F^3}{2}. \qquad (21)$$

We denote with φ and θ the azimuthal and polar angles with respect to the ellipsoid rotation axis z, respectively. Note here that only diagonal terms with $\upsilon_\alpha = \upsilon_\beta = \upsilon$ are retained after integration over all angles. As one can see from Eq. (18), the conductivity becomes scalar quantity in this approximation.

In the general case of an ellipsoidal-shaped MN, the electric conductivity is the tensor quantity (Eq. (16)). Integrating it over all nanoparticle coordinates in a solid angle $d\Omega = \sin\theta\, d\varphi\, d\theta$ gives (see Appendix)

$$\frac{1}{V} \iiint\limits_V d^3 r' \left[1 - e^{-(\nu - i\omega)t'(\mathbf{r}', \upsilon')}\right] = \frac{3}{4}\Psi(\omega, \upsilon'). \qquad (22)$$

The complex Ψ function entering in Eq. (22), has the form

$$\Psi(\omega, \upsilon') = \Phi(\omega, \upsilon') - \frac{4}{q^2}\left(1 + \frac{1}{q}\right) e^{-q}, \qquad (23)$$

with

$$\Phi(\omega, \upsilon') = \frac{4}{3} - \frac{2}{q} + \frac{4}{q^3}, \quad q \equiv q(\omega, \upsilon') = \frac{2R}{\upsilon'}(\nu - i\omega), \qquad (24)$$

and υ' $(= \varsigma\upsilon)$ is a "deformed" electron velocity[17] with the "deformation" coefficient $\varsigma_j = R/d_j$. The last summand in Eq. (23) represents the oscillation part of the Ψ function and the first one refers to its smooth part.

Accounting of Eq. (22) and only diagonal components in Eq. (16), it remains the integrals over all electron velocities. To calculate them, we pass to the spherical coordinate system with a z axis directed along the rotation axis of the spheroid (as we have done it above). Then Eq. (16) can be rewritten as

$$\begin{aligned} \sigma_{jj}(\omega) &= \frac{3e^2 m^3}{2(2\pi\hbar)^3} \frac{1}{\nu - i\omega} \int\limits_0^{2\pi} d\varphi \int\limits_0^{\pi} \sin\theta\, d\theta \\ &\times \int\limits_0^{\infty} \upsilon^2 d\upsilon\, \upsilon_j^2 \left(-\frac{\partial f_0}{\partial \varepsilon}\right) \Psi(\omega, \upsilon'), \qquad (25) \end{aligned}$$

where υ_j is the j-th component of the electron velocity, $j = x, y, z$, with

$$\begin{cases} \upsilon^2_{\binom{x}{y}} = \upsilon^2 \sin^2\theta \cdot \binom{\cos^2\varphi}{\sin^2\varphi}, \\ \upsilon_z^2 = \upsilon^2 \cos^2\theta, \end{cases}$$

respectively.

It should be noted that the "deformed" electron velocity entering in Ψ function can be expressed through the electron velocity in Cartesian coordinate system as follows

$$\upsilon' = \upsilon R \sqrt{\left(\frac{\cos^2\varphi}{a^2} + \frac{\sin^2\varphi}{b^2}\right)\sin^2\theta + \frac{\cos^2\theta}{c^2}}. \qquad (26)$$

Let us suppose that the particle in the matrix is modeled as rotationally symmetric ellipsoid ($a = b \equiv R_\perp$, $c \equiv R_\|$) with the symmetry axis along the z direction. The components of an electron velocity parallel ($\upsilon_\|$) and perpendicular ($\upsilon_\perp$) to the spheroid revolution axis

$$\upsilon_\| = \upsilon_z = \upsilon \cos\theta, \quad \upsilon_\perp = \sqrt{\upsilon_x^2 + \upsilon_y^2} = \upsilon \sin\theta \tag{27}$$

play an important role in this case, and the υ' cease to depend on the angle φ.

Let us puss from an integration in Eq. (25) over electron velocities to the integration over electron energies

$$\upsilon^4 \, d\upsilon = \frac{1}{m} \left(\frac{2\varepsilon}{m} \right)^{3/2} d\varepsilon \tag{28}$$

and account for that the integrals

$$\int\limits_0^{2\pi} \cos^2\varphi = \int\limits_0^{2\pi} \sin^2\varphi = \pi. \tag{29}$$

Then, using Eqs. (25), (28), and (29), one get for main components of the complex electric conductivity tensor

$$\sigma_{xx} = \sigma_{yy} \equiv \sigma_\perp, \qquad \sigma_{zz} = \sigma_\|, \tag{30}$$

with

$$\begin{aligned} \sigma_{\binom{\|}{\perp}}(\omega) &= \frac{3e^2}{2\pi^2} \frac{\sqrt{2m}}{\hbar^3} \left[\frac{1}{\nu - i\omega} \int\limits_0^{\pi/2} \begin{pmatrix} \cos\theta' \sin^2\theta' \\ \frac{1}{2}\cos^3\theta' \end{pmatrix} d\theta' \right. \\ &\times \left. \int_0^\infty \Psi(\omega, \varepsilon'_{\theta'}) \left(-\frac{\partial f_0}{\partial \varepsilon} \right) \varepsilon^{3/2} \, d\varepsilon \right]. \end{aligned} \tag{31}$$

We denote with $\theta' (= \theta - \pi/2)$ the angle between the direction of an electron velocity and an axis perpendicular to the spheroid rotation axes. Here and below, the upper (lower) symbol in the parentheses on the left-hand side of Eq. (31) corresponds to the upper (lower) expression in the parentheses on the right-hand side of this equation.

The Ψ function in Eq. (31) depends now on both the energy ε' and the angle θ' because the parameter q [see Eqs. (24) and (26)] for a spheroidal particle becomes dependent on the angle θ and can be determined as

$$q = \sqrt{\frac{2m}{\varepsilon}} \frac{\nu - i\omega}{\sqrt{\frac{\sin^2\theta}{R_\perp^2} + \frac{\cos^2\theta}{R_\|^2}}} \equiv q(\theta, \varepsilon), \tag{32}$$

where $R_\|$ and $R_\perp$ are the semiaxes of the spheroid. The electron energy ε' entering into the Ψ function, becomes dependent on angle θ too and for a spheroid can be presented as

$$\varepsilon'_{\theta'} = \varepsilon R^2 \left(\frac{\cos^2\theta'}{R_\perp^2} + \frac{\sin^2\theta'}{R_\|^2} \right), \tag{33}$$

where Eq. (26) was used. Because the spheroid semiaxes $R_\perp$ and $R_\|$ can be easily expressed through the radius of sphere R of an equivalent volume

$$R_\perp = R \left(\frac{R_\perp}{R_\|} \right)^{1/3}, \qquad R_\| = R \left(\frac{R_\perp}{R_\|} \right)^{-2/3}, \tag{34}$$

the energy ε' does not depend on the particle radius R but depends only on the spheroid axes ratio.

If we limited ourselves here with the case of low temperatures, then Eq. (20) can be applied, and we found

$$\int_0^\infty \Psi(\omega, \varepsilon'_{\theta'}) \, \delta(\varepsilon - \varepsilon_F) \, \varepsilon^{3/2} \, d\varepsilon = \mu_0^{3/2} \Psi(\omega, \mu'_{\theta'}), \tag{35}$$

where μ_0 is the chemical potential at zero temperature. Substituting Eq. (35) into Eq. (31) and accounting that the electron concentration at $T = 0$ can be presented as

$$n_0 = \frac{(2m\mu_0)^{3/2}}{3\pi^2\hbar^3}, \tag{36}$$

it is easy to check that Eq. (31) transforms to the form known from, e.g., Ref. 42.

A. Conductivity of a spherical MN

For particles with a spherical shape, the electric conductivity becomes a scalar quantity, and one can put $R_\| = R_\perp \equiv R$, $\varepsilon' = \varepsilon$ in Eqs. (32) and (28); then q and the Ψ function cease to dependent on the angle θ',

$$\int\limits_0^{\pi/2} \begin{pmatrix} \cos\theta' \sin^2\theta' \\ \frac{1}{2}\cos^3\theta' \end{pmatrix} d\theta' = \frac{1}{3}, \tag{37}$$

and Eq. (31) reduces to the form

$$\sigma_{sph}(\omega) = \frac{e^2\sqrt{2m}}{2\pi^2\hbar^3(\nu - i\omega)} \int_0^\infty \Psi(\omega, \varepsilon) \left(-\frac{\partial f_0}{\partial \varepsilon} \right) \varepsilon^{3/2} \, d\varepsilon. \tag{38}$$

Let us make the following change of variables in Eq. (38)

$$\eta = \frac{\varepsilon - \mu(T)}{k_B T}, \qquad d\eta = \frac{d\varepsilon}{k_B T}. \tag{39}$$

Then

$$-\frac{\partial f_0}{\partial \varepsilon} = \frac{e^{-\eta}}{(1 + e^{-\eta})^2} d\eta, \tag{40}$$

and the integral in Eq. (38) can be presented as

$$\int\limits_{-\mu/(k_B T)}^{\infty} \Psi(\omega, \eta) \, (\mu + \eta k_B T)^{3/2} \frac{e^{-\eta}}{(1 + e^{-\eta})^2} \, d\eta \equiv I, \tag{41}$$

where

$$\Psi(\omega,\eta)=\frac{4}{3}-\frac{\sqrt{\frac{2}{m}(\mu+\eta kT)}}{R(\nu-i\omega)}+\frac{[\frac{2}{m}(\mu+\eta kT)]^{3/2}}{2R^3(\nu-i\omega)^3}$$
$$-\ \frac{\frac{2}{m}(\mu+\eta kT)}{R^2(\nu-i\omega)^2}\left(1+\frac{\sqrt{\frac{2}{m}(\mu+\eta kT)}}{2R(\nu-i\omega)}\right)e^{-\frac{2R(\nu-i\omega)}{\sqrt{\frac{2}{m}(\mu+\eta kT)}}},\tag{42}$$

with[43]

$$\mu\equiv\mu(T)\simeq\mu_0\left[1-\frac{\pi^2}{12}\left(\frac{k_BT}{\mu_0}\right)^2\right].\tag{43}$$

Since the input of the integrand tends to zero as $\eta\to-\infty$, the lower limit in this integral can be extended to the $-\infty$. The derivative $(-\partial f_0/\partial\varepsilon)$ has a maximum at the point $\varepsilon=\mu$. So, it is conveniently to expand the product of $\Psi\cdot(\mu+\eta k_BT)^{3/2}\equiv\Xi(\eta)$ in the powers of η

$$\Xi(\eta)\simeq\mu^{3/2}\Psi(0)+\left[\frac{3}{2}k_BT\sqrt{\mu}\Psi(0)+\mu^{3/2}\Psi'(0)\right]\eta$$
$$+\ \frac{1}{8\sqrt{\mu}}\left[3(k_BT)^2\Psi(0)+12k_BT\mu\Psi'(0)+4\mu^2\Psi''(0)\right]\eta^2$$
$$+\ 0[\eta]^3,\tag{44}$$

with

$$\Psi(0)=\Psi(\omega,\eta)|_{\eta\to0},\quad \Psi'(0)=\frac{\partial}{\partial\eta}\Psi(\omega,\eta)|_{\eta\to0},$$
$$\Psi''(0)=\frac{\partial^2}{\partial\eta^2}\Psi(\omega,\eta)|_{\eta\to0}.\tag{45}$$

Note, that $\Psi(0)$ at $v'=v_F$ coincides with the $\Psi(\omega)$ defined by Eq. (23).

Then, the integral (41) can be presented as the sum of integrals

$$I\simeq\ \mu^{3/2}\Psi(0)\ I_1+\left[\frac{3}{2}k_BT\sqrt{\mu}\Psi(0)+\mu^{3/2}\Psi'(0)\right]I_2$$
$$+\ \frac{1}{2}\left[\frac{3(k_BT)^2}{4\sqrt{\mu}}\Psi(0)+3k_BT\sqrt{\mu}\Psi'(0)+\mu^{3/2}\Psi''(0)\right]I_3,\tag{46}$$

where the symbols I_1, I_2 and I_3 represent the integrals

$$I_1=\int\limits_{-\infty}^{\infty}\frac{e^{-\eta}\,d\eta}{(1+e^{-\eta})^2}=1,\quad I_2=\int\limits_{-\infty}^{\infty}\frac{\eta\,e^{-\eta}\,d\eta}{(1+e^{-\eta})^2}=0,\tag{47}$$

and

$$I_3=\int\limits_{-\infty}^{\infty}\frac{\eta^2e^{-\eta}\,d\eta}{(1+e^{-\eta})^2}=\frac{\pi^2}{6}.\tag{48}$$

Using Eqs. (39)–(48), Eq. (38) transforms into

$$\sigma_{sph}(\omega)\ =\ \frac{e^2\sqrt{2m\mu}}{2\pi^2\hbar^3(\nu-i\omega)}\left\{\mu\left[1+\frac{\pi^2}{8}\left(\frac{k_BT}{\mu}\right)^2\right]\Psi(0)\right.$$
$$\left.+\ \frac{\pi^2}{6}\left[3k_BT\ \Psi'(0)+\mu\Psi''(0)\right]+0[\eta]^3\right\}.\tag{49}$$

Here

$$\Psi'(0)\ =\frac{k_BT}{\mu q_\mu}\left[-1+\frac{6}{q_\mu^2}-\frac{6}{q_\mu}e^{-q_\mu}\left(1+\frac{1}{q_\mu}+\frac{q_\mu}{3}\right)\right],\tag{50}$$

$$\Psi''(0)\ =\frac{(k_BT)^2}{2\mu^2q_\mu}\left[1+\frac{6}{q_\mu^2}\right.$$
$$\left.-\quad 4e^{-q_\mu}\left(1+\frac{q_\mu}{2}+\frac{3}{2q_\mu}+\frac{3}{2q_\mu^2}\right)\right],\tag{51}$$

with

$$q_\mu=\frac{2R(\nu-i\omega)}{\sqrt{2\mu/m}}.\tag{52}$$

Substituting Eqs. (50)–(51) into Eq. (49), we obtain

$$\sigma_{sph}(\omega,T)\ =\ \frac{me^2\mu R}{\pi^2\hbar^3q_\mu}\left[\Psi(0)+\alpha_T\Psi_T(\omega)\right],\tag{53}$$

with

$$\alpha_T=\frac{\pi^2}{6}\left(\frac{k_BT}{\mu}\right)^2,\tag{54}$$

$$\Psi_T(\omega)=\Phi_T(\omega)-\left[1+\frac{8}{q_\mu}+\frac{24}{q_\mu^2}\left(1+\frac{1}{q_\mu}\right)\right]e^{-q_\mu},\tag{55}$$

$$\Phi_T(\omega)=1-\frac{4}{q_\mu}+\frac{24}{q_\mu^3}.\tag{56}$$

When the temperature $T\to0$ in Eq. (54), then Eq. (53) is reduced to the form

$$\sigma_{sph}(\omega)=\frac{e^2\mu_0^{3/2}\sqrt{2m}}{2\pi^2\hbar^3}\frac{\Psi(0)}{\nu-i\omega},\tag{57}$$

known from other calculations (see, e.g., Ref. 44).

The conductivity of MN given by Eq. (53) is a complex value. Practically, we need to know both the real and the imaginary parts of it.

Further analytical calculations are possible for some particular cases. In the case of a spherical MN there are three actual frequencies that are considered usually: the frequency of an incident electromagnetic field ω, the collision frequency of electrons in the particle volume ν, and the vibration frequency between the particle walls

$\nu_s = v_F/(2R)$ (if the particle size is less than the electron mean free path). When $\nu > \nu_s$, the mechanism of an electron scattering in the bulk is dominated, and an electron scattering from the particle surface gives only small corrections of the order of ν_s/ν. But we are interested in the case when the mechanism of the surface electron scattering dominates, which corresponds to $\nu < \nu_s$.

Let us suppose that the mean free path of a conduction electron l is much greater than the particle size. In this case, an electron scattering occurs mainly from the inner surface of the MN. The electrons oscillate between the walls of the particle with the frequency ν_s. We restrict ourselves here only to the case, when $\nu \ll \nu_s$. In this limit case, to a first approximation, formally one can put $\nu \to 0$. If one introduce the designation

$$q_i = \frac{\omega}{\nu_s}, \tag{58}$$

then for the real and the imaginary parts of the ratios $\Psi/(\nu - i\omega)$ and $\Psi_T/(\nu - i\omega)$, we obtain

$$\mathrm{Re}\left[\frac{\Psi}{\nu - \mathrm{i}\omega}\right]_{\nu\to 0} = \frac{1}{\omega}\left[\frac{2}{\mathrm{q_i}} - \frac{4}{\mathrm{q_i^2}}\sin\mathrm{q_i} + \frac{4}{\mathrm{q_i^3}}(1 - \cos\mathrm{q_i})\right], \tag{59}$$

$$\mathrm{Im}\left[\frac{\Psi}{\nu - \mathrm{i}\omega}\right]_{\nu\to 0} = \frac{4}{\omega}\left[\frac{1}{3} + \frac{1}{\mathrm{q_i^2}}\left(\cos\mathrm{q_i} - \frac{\sin\mathrm{q_i}}{\mathrm{q_i}}\right)\right], \tag{60}$$

and

$$\begin{aligned}\mathrm{Re}\left[\frac{\Psi_\mathrm{T}}{\nu - \mathrm{i}\omega}\right]_{\nu\to 0} &= \frac{1}{\omega}\left[\left(1 - \frac{24}{\mathrm{q_i^2}}\right)\sin\mathrm{q_i}\right.\\ &+ \left.\frac{4}{q_i}\left(1 + \frac{6}{q_i^2}\right) + \frac{8}{q_i}\left(1 - \frac{3}{q_i^2}\right)\cos q_i\right],\end{aligned} \tag{61}$$

$$\begin{aligned}\mathrm{Im}\left[\frac{\Psi_\mathrm{T}}{\nu - \mathrm{i}\omega}\right]_{\nu\to 0} &= \frac{1}{\omega}\left[1 - \left(1 - \frac{24}{q_i^2}\right)\cos q_i\right.\\ &+ \left.\frac{8}{q_i}\left(1 - \frac{3}{q_i^2}\right)\sin q_i\right].\end{aligned} \tag{62}$$

Substituting Eqs. (59)–(62) into Eq. (53), one obtains for the real and imaginary parts of σ the following expressions:

$$\begin{aligned}\sigma'_{sph}(\omega, T) &= \frac{3}{4}\frac{e^2 n_e(T)}{m\omega}\left\{\frac{2}{q_i} - \frac{4}{q_i^2}\sin q_i + \frac{4}{q_i^3}(1 - \cos q_i)\right.\\ &+ \left.\alpha_T\left[\frac{4}{q_i} + \frac{24}{q_i^3} + \left(1 - \frac{24}{q_i^2}\right)\sin q_i + \frac{8}{q_i}\left(1 - \frac{3}{q_i^2}\right)\cos q_i\right]\right\}\end{aligned} \tag{63}$$

$$\begin{aligned}\sigma''_{sph}(\omega, T) &= \frac{3}{4}\frac{e^2 n_e(T)}{m\omega}\left\{\frac{4}{3} + \frac{4}{q_i^2}\left(\cos q_i - \frac{\sin q_i}{q_i}\right)\right.\\ &+ \left.\alpha_T\left[1 + \frac{8}{q_i}\left(1 - \frac{3}{q_i^2}\right)\sin q_i - \left(1 - \frac{24}{q_i^2}\right)\cos q_i\right]\right\},\end{aligned} \tag{64}$$

provided that $\nu \ll \nu_s$. In these equations the electron concentration depends on the temperature as[43]

$$n_e(T) = n_0\left[1 + \frac{\pi^2}{8}\left(\frac{k_B T}{\mu(T)}\right)^2\right]. \tag{65}$$

If one neglect the oscillation terms in Eq. (64) then we obtain

$$\sigma''_{sph}(\omega, T) \simeq \frac{\omega_{pl}^2(T)}{4\pi\omega}\left(1 + \frac{3}{4}\alpha_T\right), \tag{66}$$

with $\omega_{pl}^2(T) = 4\pi e^2 n_e(T)/m$.

At $T \to 0$, Eqs. (63) and (64) agree with expressions known from an earlier calculations.[42,44]

Another simplest calculations of conductivity tensor in the case of MNs with spherical shape can be made in approximation of $\nu_s \gg \nu$ with the help of the following formulas

$$\begin{aligned}\sigma'(\omega, T) &= \frac{e^2}{\pi^2}\frac{\mu(T)}{\omega v_F \hbar^3}\left\{\int_0^\infty d\varepsilon\left(-\frac{\partial f_0}{\partial\varepsilon}\right)\varepsilon^{3/2}\right.\\ &\times \left.\left[\frac{2}{q_\varepsilon} - \frac{4}{q_\varepsilon^2}\sin q_\varepsilon + \frac{4}{q_\varepsilon^3}(1 - \cos q_\varepsilon)\right]\right\},\end{aligned} \tag{67}$$

$$\begin{aligned}\sigma''(\omega, T) &= \frac{4e^2}{\pi^2}\frac{\mu(T)}{\omega v_F \hbar^3}\left\{\int_0^\infty d\varepsilon\left(-\frac{\partial f_0}{\partial\varepsilon}\right)\varepsilon^{3/2}\right.\\ &\times \left.\left[\frac{1}{3} + \frac{1}{q_\varepsilon^2}\left(\cos q_\varepsilon - \frac{1}{q_\varepsilon}\sin q_\varepsilon\right)\right]\right\}.\end{aligned} \tag{68}$$

The parameter q_ε, (defined by Eq. (52) with $\mu = \varepsilon$), is governed by the frequency. Depending on the ratio between the incident frequency and the frequency ν_s, the value of q_ε can be greater or less than 1. To perform subsequent analytical calculations of the integrals involved into Eqs. (67) and (68), one may use the same method as one described above after Eq. (38). Applying it, one comes to the results given above by Eqs. (63) and 64).

B. Linewidth and "figure of merit"

The linewidth of the particle-plasmon resonance is controlled by lifetime broadening due to various decay processes. Knowing the expressions for conductivity tensor Eq. (31) and Eq. (63), the halfwidth of the plasmon line absorption can be easy calculated by means of relation

$$\Gamma_j(\omega, T) = \frac{4\pi}{\epsilon_\infty + n^2(1/L_j - 1)}\mathrm{Re}\,\sigma_{jj}(\omega, T), \tag{69}$$

where $n(=\sqrt{\epsilon_m})$ is the refractive index of the surrounding media and $\varepsilon_\infty \equiv 1 + \epsilon_{\mathrm{inter}}$ is the high frequency dielectric constant due to interband and core transitions of the inner electrons in a MN's material.

The "figure of merit" can be expressed through the σ_{jj} as well. For MNs with spheroidal shape we found[44]

$$\mathrm{FOM}_{\left({\parallel \atop \perp}\right)} = \frac{n\omega_{\mathrm{pl}}(1/L_{\left({\parallel \atop \perp}\right)} - 1)}{4\pi\sqrt{\varepsilon_\infty + (1/L_{\left({\parallel \atop \perp}\right)} - 1)n^2}}\sigma'^{-1}_{\left({\parallel \atop \perp}\right)}(\omega, T), \quad (70)$$

with geometrical factors[45]

$$L_\parallel = \frac{1}{(1 + R_\parallel/R_\perp)^{1.6}} \qquad L_\perp = \frac{1}{2}(1 - L_\parallel). \quad (71)$$

Finally, it should be reminded that the real and imaginary parts of a dielectric constant tensor ϵ_{jj} can be easily obtained with help of tensor σ_{jj}, as[43]

$$\epsilon'_{jj}(\omega, T) = \epsilon_\infty - \frac{4\pi}{\omega}\sigma''_{jj}(\omega, T), \quad (72)$$

$$\epsilon''_{jj}(\omega, T) = \frac{4\pi}{\omega}\sigma'_{jj}(\omega, T). \quad (73)$$

The sign in the last equation and before second term in Eq. (72) is defined by sign in time dependence of an external electric field $\mathbf{E}(t) = \mathbf{E}_0 e^{-i\omega t}$. The imaginary part of the dielectric constant will lead principally to a damping and broadening of SPR.

The linewidth of SPR and FOM are strongly dependent on the particle radius. We will illustrate this dependence below building the temperature behavior of SPR linewidth for different R as an example.

The SPR line width is plotted in Fig. 1 against temperature for spherical Au nanoparticles with two different radii, embedded in the water ($n = 1.33$). Calculations were done according to the formulas Eq. (69) and (63) for the following parameters of Au nanoparticle:[46] $v_F = 1.394\times10^8$ cm/s, $T_F = 6.41\times10^4$ K, $\omega_{\mathrm{pl}} = 1.37\times10^{16}\ \mathrm{s}^{-1}$, and $\epsilon_\infty = 9.84$. The electron concentration was estimated from Eq. (65) with n_0 given above by Eq. (36). For Au, $n_0 \simeq 5.9 \times 10^{22}\ \mathrm{cm}^{-3}$. The behavior of $\Gamma(T)$ is governed by the temperature dependence of the $\epsilon''(T)$ in accordance with Eqs. (69) and (73).

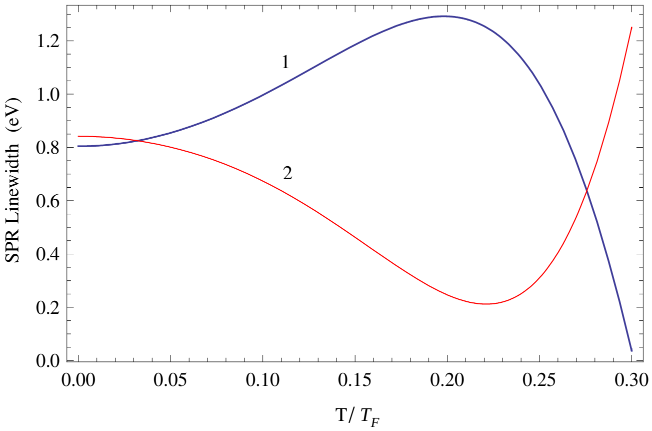

FIG. 1. (Color online) SPR linewidth vs temperature for spherical Au particles with different R ($\AA$): 50 (1) and 54.7 (2), embedded in water.

The high temperature of an electron gas can be achieved inside of MN with using laser pumping at SPR frequency when the hot electrons are produced. As the temperature of an electron gas is decreased after an initial excitation, the SPR linewidth can increased (see curve 1, Fig. 1) or decreased (curve 2), depending on the particle radius. Such different behavior is due to the linewidth oscillations with the particle radius changing.[44] Earlier[27,30], the results for Ag and Au nanoparticles were reported when the linewidth is only reduced linearly with the temperature lowering over a range of a crystal temperatures.

Let us calculate the polarizability tensor for MNs at finite temperatures.

IV. POLARIZABILITY TENSOR

The dipole electric moment for a spherical particle embedded in the media with dielectric constant ϵ_m, can be written as

$$d_j(\omega) = \epsilon_m \sum_{k=1}^{3} \alpha_{jk}(\omega)\, E_k(\omega), \quad (74)$$

where E_k is the k component of an external electric field and α_{jk} is the polarizability tensor of the MN. The calculation of $\mathbf{d}$ is especially simple for the case, when the particle sizes are small comparing to the some "wave length" $\delta \sim c/(\sqrt{|\epsilon|}\ \omega)$, which corresponds to the frequency ω in the particle bulk. In this case one can calculate the polarizability of MN using the formulae obtained for an external uniform statical field. In general terms this tensor can be treated as being complex value

$$\alpha_{jk}(\omega) = \alpha'_{jk}(\omega) + i\alpha''_{jk}(\omega). \quad (75)$$

Tensor of an electric conductivity was introduced by Eq. (15). The component of an inner electric field in Eq. (15) is connected to a component of an external electric in Eq. (74) field by expression (3). Because, the density of electric current is related with the dipole moment by a simple relation

$$j(t) = \frac{1}{V}\frac{\partial}{\partial t}d(t), \quad (76)$$

it is easy to establish the connection between polarizability and conductivity of MN. Performing the Fourier transformation of Eq. (76), we obtain

$$j(\omega) = \frac{i\omega}{V}\, d(\omega). \quad (77)$$

Then, using Eqs. (74), (77), and (15), the polarizability tensor can be expressed through the conductivity tensor α_{jj} by means of

$$\alpha_{jj}(\omega, T) = -\frac{V}{\epsilon_m\omega}\frac{i\,\sigma_{jj}(\omega, T)}{1 + L_j[\epsilon_{jj}(\omega)/\epsilon_m - 1]}. \quad (78)$$

Parameter V in Eq. (78) represents for MN with a spheroidal shape, the volume of spheroid ($=\frac{4}{3}\pi R_{\perp}^{2} R_{\parallel}$).

Using Eqs. (72) and (73) for an isolated MN *in host*, we get the Clausius-Mossotti dipole polarizability[1]

$$\alpha_{jj}(\omega, T) = \frac{V}{4\pi L_j} \frac{\epsilon_{jj}(\omega, T) - \epsilon_m}{\epsilon_{jj}(\omega, T) + (1/L_j - 1)\epsilon_m}, \tag{79}$$

where the tensor ϵ_{jj} would correspond to a given frequency ω, and in the case of frequencies close to the plasma oscillations of electrons in metal, can be presented as

$$\epsilon_{jj}(\omega, T) \simeq \epsilon_{\infty} - \left(\frac{\omega_{\rm pl}}{\omega}\right)^2 + \frac{4\pi}{\omega} i\sigma_{jj}(\omega, T). \tag{80}$$

Optical absorption generally measures $\operatorname{Im}\epsilon(\omega, T)$.

V. LIGHT ABSORPTION AND SCATTERING

In classical electrodynamic it is supposed that the light scattering results from the polarization of the scattered particle when it is illuminated with a beam of light. Because the spatially uniform field causes only a dipole polarization, the nanoparticle scatters the light like as a vibration dipole.[1] In the case of particles of a *spheroidal shape*, the dipole moment of the MN can be presented in the form[47]

$$\mathbf{d} = \alpha_{\perp}\mathbf{E} + (\alpha_{\parallel} - \alpha_{\perp})(\mathbf{m}\cdot\mathbf{E})\mathbf{m}, \tag{81}$$

where $\mathbf{m}$ is the unit vector directed along the spheroid axis of revolution. Accounting for that the $\mathbf{m}\cdot\mathbf{E} = E\cos\phi$, where ϕ is the angle between the spheroid axis of revolution and the direction of an electric field $\mathbf{E}$,

$$\mathbf{d} = \sqrt{\alpha_{\perp}^2 \sin^2\phi + \alpha_{\parallel}^2 \cos^2\phi}\;\mathbf{E}. \tag{82}$$

Using our forerunning formulae for $\mathbf{d}$ and α, the temperature dependence of light absorption and scattering can be calculated. The overall absorption and scattering cross-sections for a spheroidal MN can presented as[47]

$$C_{abs} = 4\pi\frac{\omega}{c}\sqrt{\epsilon_m}\left[(\operatorname{Im}\alpha_{\parallel})\cos^2\phi + (\operatorname{Im}\alpha_{\perp})\sin^2\phi\right], \tag{83}$$

$$C_{sca} = \frac{8}{3}\pi\left(\frac{\omega}{c}\sqrt{\epsilon_m}\right)^4\left(|\alpha_{\parallel}|^2\cos^2\phi + |\alpha_{\perp}|^2\sin^2\phi\right). \tag{84}$$

The square of diagonal components of the polarizability tensor can be presented in the Lorenzian form as

$$|\alpha_{\binom{\parallel}{\perp}}|^2 = \left(\frac{V}{4\pi L_{\binom{\parallel}{\perp}}}\right)^2 \frac{\left((1-\xi_m)\omega^2 - \omega_{\binom{\parallel}{\perp}}^2\right)^2 + \left(2\omega\gamma_{\binom{\parallel}{\perp}}\right)^2}{\left(\omega^2 - \omega_{\binom{\parallel}{\perp}}^2\right)^2 + \left(2\omega\gamma_{\binom{\parallel}{\perp}}\right)^2}, \tag{85}$$

and the imaginary part of the polarizability tensor is

$$\operatorname{Im}\alpha_{\binom{\parallel}{\perp}} = \left(\frac{V}{4\pi L_{\binom{\parallel}{\perp}}}\right)\frac{2\omega^3\xi_m\gamma_{\binom{\parallel}{\perp}}}{\left(\omega^2 - \omega_{\binom{\parallel}{\perp}}^2\right)^2 + \left(2\omega\gamma_{\binom{\parallel}{\perp}}\right)^2}. \tag{86}$$

Here

$$\xi_m = \frac{\epsilon_m}{\epsilon_m + L_{\binom{\parallel}{\perp}}(1-\epsilon_m)}, \tag{87}$$

$$\omega_{\binom{\parallel}{\perp}}^2 \equiv \omega_{\binom{\parallel}{\perp}}^2(T) = \frac{L_{\binom{\parallel}{\perp}}}{\epsilon_m + L_{\binom{\parallel}{\perp}}(1-\epsilon_m)}\,\omega_{pl}^2(T) \tag{88}$$

is the $\parallel$ and $\perp$ surface plasmon frequencies, and

$$\gamma_{\binom{\parallel}{\perp}} \equiv \gamma_{\binom{\parallel}{\perp}}(\omega, T) = \frac{2\pi L_{\binom{\parallel}{\perp}}}{\epsilon_m + L_{\binom{\parallel}{\perp}}(1-\epsilon_m)}\operatorname{Re}\sigma_{\binom{\parallel}{\perp}}(\omega, T) \tag{89}$$

is the half-width of the resonance for light polarized along ($\parallel$) or across ($\perp$) the rotation axis of the spheroid, $\sigma_{\parallel}$, $\sigma_{\perp}$ are the corresponding components of the conductivity tensor, and $L_{\parallel}$, $L_{\perp}$ are the geometrical factors given above by Eqs. (71).

On resonance, the polarizability tensor looks as

$$\alpha_{\binom{\parallel}{\perp}}(\omega, T) \simeq \frac{V}{8\pi}\frac{\xi_m\omega_{\binom{\parallel}{\perp}}(T)}{L_{\binom{\parallel}{\perp}}\gamma_{\binom{\parallel}{\perp}}(\omega, T)}, \tag{90}$$

with $\gamma_{\binom{\parallel}{\perp}}$ taken at $\omega = \omega_{\binom{\parallel}{\perp}}$. The contribution of non-resonant frequencies is so small that their input into the scattering cross section can be neglected.

In the case of MN with a spherical shape $L_{\parallel} = L_{\perp} = 1/3$, and Eqs. (87)–(89) become the forms

$$\xi_m = \frac{3\epsilon_m}{2\epsilon_m + 1}, \tag{91}$$

$$\omega_{\binom{\parallel}{\perp}}^2(T) \equiv \omega_{sp} = \frac{\omega_{pl}^2(T)}{2\epsilon_m + 1}, \tag{92}$$

$$\gamma_{\binom{\parallel}{\perp}}(\omega, T) \equiv \gamma_{sp}(\omega, T) = \frac{2\pi}{2\epsilon_m + 1}\,\sigma(\omega, T). \tag{93}$$

Then the expressions (84) and (83) can be easily transformed to the forms

$$C_{abs}(\omega, T) = 9V\varepsilon_m^{3/2}\frac{\omega}{c}\frac{\epsilon''(\omega, T)}{[\epsilon'(\omega, T) + 2\epsilon_m]^2 + [\epsilon''(\omega, T)]^2}, \tag{94}$$

$$C_{sca}(\omega, T) = \frac{3V^2}{2\pi}\epsilon_m^2\left(\frac{\omega}{c}\right)^4\frac{[\epsilon'(\omega, T) - \epsilon_m]^2 + [\epsilon''(\omega, T)]^2}{[\epsilon'(\omega, T) + 2\epsilon_m]^2 + [\epsilon''(\omega, T)]^2}, \tag{95}$$

where we have combined Eqs. (91)–(93) with the real and imaginary parts of Eq. (80). The most intense cross-sections are observed at the frequency which corresponds to the plasmon resonance of a *spherical* nanoparticle in the vacuum. Formulae (95) and Eq. (94) yield a resonance when $\epsilon'(\omega, T) = -2\epsilon_m$. The absorption and the scattering cross-section defined by Eqs. (83) and (84) reach the maximal values, as well, at the frequencies of the SPRs $\omega = \omega_{\left(\substack{\parallel \\ \perp}\right)}$. Near the surface plasmon resonance, light may interact with the particle over a cross-sectional area usually (at low temperatures) larger than the geometric cross section of the particle because the polarizability of the particle becomes very high in this frequency range.

We will calculate the the scattering efficiency of the MN, which we define as the ratio

$$S_{ef} = \frac{C}{C_{geom}}, \qquad C_{geom} = \pi \left(\frac{c}{\omega_{pl}} \right)^2, \qquad (96)$$

where C_{geom} is the geometrical cross-section of an individual particle and C is defined by Eqs. (83) and (84) or by Eqs. (94) and (95).

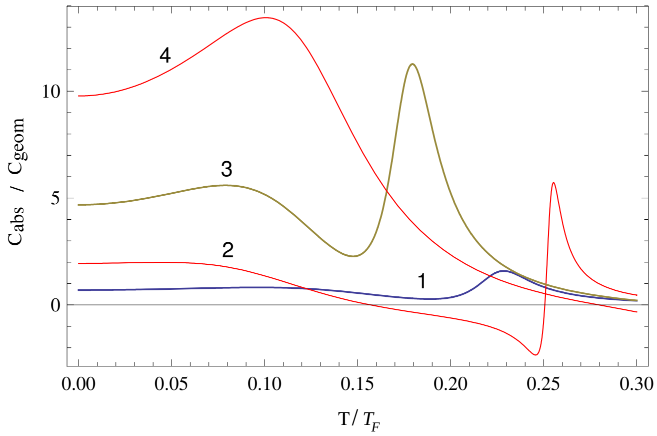

FIG. 2. (Color online) The absorption crossection vs temperature for spherical Au particles with different R ($\AA$): 78 (1), 100 (2), 125 (3), and 150 (4), embedded in water.

Figure 2 shows the variation of an absorption efficiency as a function of temperature for a gold nanoparticles with a spherical shape embedded in the water ($n = 1.33$). The calculations were performed in an accordance with Eqs. (96) and (94), with the use of the same parameters as above for Fig. 1. For zero temperature we get the classical result,[1,2] when the SPR intensity depends on the particle radius: larger particles have a larger scattering or absorption cross sections. The situation is drastically changed at finite electron temperatures. As can see from Figure 2, the absorption efficiency can not only increased (right hand sides of curves 1–4) with temperature decreasing, but decreases as well (left hand sides of curves 1–4). We have an interesting situation, when the absorption crossection with the temperature lowering is increased at first, reaches its peak, then is decreased, and start to increase again. These observations are explained with the conductivity of MN, which oscillate with particle radius changing.[42]

In the case of light scattering (see Fig. 3), the effect of MN size is more pronounced because the scattering cross-section is proportional to the square of a particle volume.

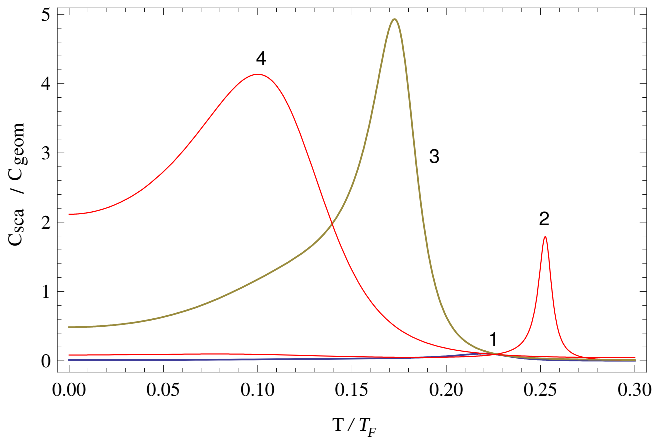

FIG. 3. (Color online) The same as in Fig. 2, but for scattering crossection.

From Fig. 3, one can see that the efficiency of light scattering at resonance frequency has not only increased (curves 1–3) with the enhancement of the MN radius, but can be decreased (curve 4) as well. The latter means that the efficiency of scattering at resonance frequency can be suppressed with temperature rise for some particle radiuses. Depending on the electron temperature, the scattering efficiency reaches the maximum value, the peak position of which depends on the nanoparticle radius.

The peak positions of the resonance plasmon absorption (or scattering) by Au nanoparticle embedded in water can shifted toward the shorter wavelengths as the temperature of electron gas is lowered after an initial excitation. This behavior is consistent with the known temperature-dependent shift of the differential transmission peak in isolated sodium nanoparticle.[23]

VI. DISCUSSION OF RESULTS

Here we discuss shortly the effects caused by deviations from the spherical particle shape. When the symmetry of the particle decreases, the number of resonance peaks increases. If the shape of particle deviates from spherical one, the 3-fold degeneracy dipole mode split into two (for spheroid) or three (for ellipsoid) modes giving rise to correspondent scattering peaks. In this case the plasmon response depends strongly on the particle position relative to the illumination direction. To evaluate the electron temperature effect on the absorption or scattering crossections for various illumination directions, one can perform a numerical calculations with the use of Eqs. (83)–(89) and Eq. (31).

The particle absorption or scattering effects depend on the size and shape of the individual particles. Metallic particles that are much smaller than the wavelength of light tend to absorb more and hence absorption is dominated. The scattered light intensity from small MNs is extremely low. Indeed, Rayleigh scattering theory predicts that the scattering cross section of a spherical cluster should drop as the sixth power of the diameter.

The quantity that is measured experimentally is frequency-resolved time-dependent transmission[23] Υ_{on} after the exitation of the MN by a pump laser pulse. Then, the static equilibrium transmission Υ_{off} of the sample measured in the absence of the pump is subtracted to obtain the relative differential transmission[19] $\delta\Upsilon/\Upsilon = (\Upsilon_{on} - \Upsilon_{off})/\Upsilon_{off}$. In the thermal equilibrium, the $\delta\Upsilon$ can be related to the temperature dependent absorption cross section by[34]

$$\frac{\delta\Upsilon}{\Upsilon} = -\frac{3}{2\pi R^2}\left[C_{abs}(\omega, T) - C_{abs}(\omega, T_0)\right], \qquad (97)$$

where T_0 is the temperature of of the MN before excitation. This relation holds for very small sizes of MN when the reflectivity of the MN is very small.

A direct comparison of theoretical results with most of the available experimental measurements of the optical properties of MNs is still a matter of debate because inhomogeneities in nanoparticle size, shape, and local environment hide the homogeneous width of the surface plasmon resonance.

VII. CONCLUSIONS

We have applied a kinetic theory to calculate the optical properties of a metal nanoparticle embedded in a dielectric media at different temperatures. It allows to determine the cross-section of light absorption or scattering for various polarizations of the incident electromagnetic wave. The obtained analytical formulas provides to evaluate the dynamic of a light absorption or scattering intensities at the plasmon frequencies for nanoparticles with different radii and shapes, when the temperature of electron gas becomes settle after an action of a laser pulse.

The analytical expressions for electroconductivity and polarizability tensors have been obtained for the case of MNs with a spherical shape. They allow to calculate the number other physical quantities (e.g., resonance linewidth, figure of merit etc) for a given temperature. We studied theoretically the variation of both the linewidth of SPR and the efficiency of the light absorption and scattering by MN with changing of the electron temperature. The case where the frequency of a laser beam is close to surface plasmon frequencies of a spheroidal MN is studied in detail.

The high sensitivity of the temperature dependence of SPR linewidth to the radius of a particle was established. Even small variation in the particle radius can drastically change the run of the SPR linewidth curve vs temperature. This is due to the linewidth oscillations when the radius of MN is varied. The efficiencies of light absorption and scattering for various temperatures strongly depend on the particle radius as well. The Au nanoparticles with different radii are used for illustration.

Acknowledgment

The author is indebted to Prof. P. Tomchuk for useful comments and helpful discussions.

Appendix A

Below we advance the values for the integrals appeared in calculations of Eq. (22), Sec. III:

$$\int_{-1}^{1} dz\, e^{-\left(az^2+bz\right)} = \frac{1}{2}\sqrt{\frac{\pi}{a}}\left[\mathrm{Erf}\left(\frac{\mathrm{b}+2\mathrm{a}}{2\sqrt{\mathrm{a}}}\right) - \mathrm{Erf}\left(\frac{\mathrm{b}-2\mathrm{a}}{2\sqrt{\mathrm{a}}}\right)\right] e^{-\left(\frac{b^2}{4a}\right)}. \qquad (A1)$$

$$\int_{0}^{\infty} dz\, z^2 e^{-\left(z+\frac{a}{z}\right)^2} = \frac{\sqrt{\pi}}{4}(1+2a)\, e^{-4a}, \qquad (A2)$$

provided that $-\pi/4 < a < \pi/4$.

$$\int_{0}^{\infty} dz\, z^3\, \mathrm{Erfc}\Big(z+\frac{a}{z}\Big) = \frac{1}{4}\left(a+\frac{3}{4}\right) e^{-4a}, \qquad (A3)$$

provided that $\mathrm{Re}\, a > 0$.

$$\int_{0}^{\infty} dz\, z^3\, \mathrm{Erfc}\Big(z-\frac{a}{z}\Big) = \frac{1}{2}\left(a^2+a+\frac{3}{8}\right). \qquad (A4)$$

---

[1] C.F. Bohren and D.R. Huffman, *Absorption and Scattering of Light by Small Particles* (Wiley, Weinheim, 2004).

[2] U. Kreibig and M. Vollmer, *Optical Properties of Metal*

Clusters (Springer Verlag, Berlin, Heidelberg 1995).

[3] S. Nie and S.R. Emory, Science **275**, 1102 (1997).

[4] U. Schroter and A. Dereux, *Phys. Rev. B* **64**, 125420 (2001).

[5] C. Hubert, A. Rumyantseva, G. Lerondel, J. Grand, S. Kostcheev, L. Billot, A. Vial, R. Bachelot, and P. Royer, Nano Lett. **5**, 615 (2005).

[6] E. Fort and S. Gresillon, J. Phys. D: Appl. Phys. **41**, 013001 (2008).

[7] J. Jung, T. Sondergaard, S.I. Bozhevolnyi, Phys. Rev. B **76**, 035434 (2007).

[8] X. Huang, P.K. Jain, I.H. El Sayed, and M.A. El Sayed, Nanomedicine, **2**, 681 (2007).

[9] G.V. Hartland, Ann. Rev. Phys. Chem. **57**, 403 (2006).

[10] W. Cai, J.S. White, M.L. Brongersma, Nano Lett. **9**, 4403 (2009).

[11] W.A. Challener, C. Peng, A.V. Itagi, D. Karns, W. Peng, Y. Peng, X.M. Yang, X. Zhu, N.J. Gokemeijer, Y.-T. Hsia, G. Ju, R.E. Rottmayer, M.A. Seigler, E.C. Gage, Nat. Photon. **3**, 220 (2009).

[12] A. Lowery, A. Gobin, E. Day, N. Halas, J. West, Int. J. Nanomedicine, **1**, 149 (2006).

[13] L. Cao, D.N. Barsic, A.R. Guichard, M.L. Brongersma, Nano Lett. **7**, 3523 (2007).

[14] C.E. Lee, R.A. Atkins, and H.F. Taylor, Opt. Lett., **13**, 1038 (1988).

[15] J.M. Yang, H. Yang, and L. Lin, ACS NANO, **5**, 5067 (2011).

[16] J. Kinast, A. Turlapov, and J.E. Thomas, Q. Chen, J. Stajic, K. Levin, Science **307**, 1296 (2005).

[17] N.I. Grigorchuk and P.M. Tomchuk, Phys. Rev. B **84**, 085448 (2011).

[18] U. Kreibig, J. Phys. F: Metal Phys, **4**, 999, (1974).

[19] J.-Y. Bigot, J.-C. Merle, O. Cregut, and A. Daunois, Phys. Rev. Lett., **75**, 4702 (1995).

[20] M. Perner, P. Bost, U. Lemmer, G. von Plessen, J. Feldmann, U. Becker, M. Mennig, M. Schmitt, and H. Schmidt, Phys. Rev. Lett., **78**, 2192 (1997).

[21] S. Link and M.A. El-Sayed, J. Phys. Chem. B, **103**, 4212 (1999).

[22] N.J. Florous, K. Saitoh, and M. Koshiba, Optic Lett. **31**, 404 (2006); IEEE Transactions on Nanotechnology, **6**, 549 (2007); IEEE Photonics Technology Lett., **18**, 1663 (2006); **19**, 324 (2007).

[23] G. Weick, D. Weinmann, G.-L. Ingold, and R.A. Jalabert, Eur. Phys. Lett., **78**, 27002 (2007).

[24] O. Ekici, R.K. Harrison, N.J. Durr, D.S. Eversole, M. Lee, and A. Ben-Yakar, J. Phys. D: Appl. Phys., **41**, 185501 (2008).

[25] M. Liu, M. Pelton, and P. Guyot-Sionnest, Phys. Rev. B, **79**, 035418 (2009).

[26] S.-A. Biehs, O. Huth, F. Rüting, and M. Holthaus, ArXiv: 1103.4511v1 (2010).

[27] O.A. Yeshchenko, I.S. Bondarchuk, V.S. Gurin, I.M. Dmitruk, and A.V. Kotko, Surf. Sci., **608**, 275 (2012).

[28] R. Rosei, C.H. Culp, and J.H Weaver, Phys. Rev. B **10**, 484 (1974).

[29] P. Winsemius, F.F. van Kampen, H.P. Lengkeek, and C.G. van Went, J. Phys. F: Met. Phys., **6**, 1583 (1976).

[30] M. Rocca, F. Moresco, and U. Valbusa, Phys. Rev. B, **45**, 1399 (1992).

[31] R.H.M. Groeneveld, R. Sprik, and Ad Lagendijk, Phys. Rev. B, **51**, 11433 (1995).

[32] E.T. Jensen, R.E. Palmer, W. Allison, and J.F. Annett, Phys. Rev. Lett., **66**, 492 (1991).

[33] M. Maier G. Wrigge M. Astruc Hoffmann, P. Didier, and B.v. Issendorff, Phys. Rev. Lett. **96**, 117405 (2006).

[34] P.-A. Hervieux, A. Benabbas, V. Halté, and J.-Y. Bigot, Eur. Phys. J D, **24**, 185 (2003).

[35] M.I. Kaganov, I.M. Lifshitz, and L.V. Tanatarov, Zh. Eksp. Teor. Fiz., **31**, 232 (1956) [Sov. Phys.- JETP, **4**, 173 (1957)].

[36] Y. Ping, D. Hanson, I. Koslow, T. Ogitsu, D. Prendergast, E. Schwegler, G. Collins, and A. Ng, Phys. Plasmas **15**, 056303 (2008).

[37] S. Riedl, E.R. Sánchez Guajardo, C. Kohstall, A. Altmeyer, M.J. Wright, J.H. Denschlag, R. Grimm, G.M. Bruun, and H. Smith, Phys. Rev. A, **78**, 053609 (2008).

[38] C. Yannouleas and R.A. Broglia, Ann. Phys. (NY) **217**, 105 (1992).

[39] L.D. Landau and E.M. Lifshitz, *Electrodynamics of Continous Media* (Pergamon, New York, 1986).

[40] C. Cercignani, *Theory and Application of the Boltzmann Equation* (Scotish Academic, Edinburg, 1975); A.F. Alexandrov, L.C. Bogdankevich, and A.A. Rukhadze, *Principles of Plasma Electrodynamics* (Springer, Berlin, 1984).

[41] S.V. Berezkina, I.A. Kuznetsova, and A.A. Yushkanov, Zh. Tekh. Fiz. **74**, 67 (2004).

[42] N.I. Grigorchuk, J. Appl. Phys., **112**, 064306 (2012).

[43] V.G. Levich, *A course of the Theoretical Physics*, Vol. 1 (Nauka, Moskow, 1969).

[44] N.I. Grigorchuk, J. Phys. Chem. C, **116**, 23704 (2012).

[45] J. Becker, A. Trügler, A. Jakab, U. Hohenester, C. Sönnichsen, Plasmonics **5**, 161 (2010).

[46] Ch. Kittel, *Introduction to Solid State Physics* (Wiley, New York 1974).

[47] N.I. Grigorchuk, Eur. Phys. Lett., **97**, 45001 (2012).